

Article

# Effects of Thermal Annealing on Optical Properties of Be-Implanted GaN Thin Films by Spectroscopic Ellipsometry

Wenwang Wei <sup>1,2</sup>, Jiabin Wang <sup>1</sup>, Yao Liu <sup>1</sup>, Yi Peng <sup>1</sup>, Mudassar Maraj <sup>1</sup>, Biaolin Peng <sup>1</sup>, Yukun Wang <sup>1</sup> and Wenhong Sun <sup>1,3,\*</sup>

<sup>1</sup> Research Center for Optoelectronic Materials and Devices, School of Physical Science & Technology, Guangxi University, Nanning 530004, China; weiww9189@163.com (W.W.); 1907401030@st.gxu.edu.cn (J.W.); malena326@126.com (Y.L.); pengyi41@outlook.com (Y.P.); mudassar@mail.ustc.edu.cn (M.M.); pengbl8@126.com (B.P.); ykwang0929@163.com (Y.W.)

<sup>2</sup> College of Chemistry and Chemical Engineering, Guangxi University, Nanning 530004, China

<sup>3</sup> Guangxi Key Laboratory of Processing for Non-ferrous Metallic and Featured Materials, Nanning 530004, China

\* Correspondence: youzi7002@gxu.edu.cn

Received: 10 May 2020; Accepted: 25 May 2020; Published: 30 May 2020



**Abstract:** Wide bandgap III-V compounds are the key materials for the fabrication of short-wavelength optical devices and have important applications in optical displays, optical storage devices and optical communication systems. Herein, the variable-angle spectroscopic ellipsometry (SE) measurements are performed to investigate the thickness and optical properties of beryllium-implanted gallium nitride thin films that have been deposited on (0001) sapphire substrates by using low-pressure metalorganic chemical vapor deposition (LPMOCVD). The film layer details are described by using Parametric Semiconductor oscillators and Gaussian oscillators in the wavelength range of 200–1600 nm. The thickness, refractive indices and extinction coefficients of the Be-implanted films are determined at room temperature. Analysis of the absorption coefficient shows that the optical absorption edge of Be-implanted films changes from 3.328 eV to 3.083 eV in the temperature range of 300–850 K. With the variable temperature,  $E_g$  is demonstrated to follow the formula of Varshni. A dual-beam ultraviolet–visible spectrophotometer (UV–VIS) is used to study the crystal quality of samples, indicating that the quality of rapid thermal annealing (RTA) sample is better than that unannealed sample. By transport of ions in matter (TRIM) simulation and SE fitting the depths of Be implanted gallium nitride (GaN) films are estimated and in good agreement. The surface and cross-section morphologies are characterized by atomic force microscopy (AFM) and scanning electron microscope (SEM), respectively. The surface morphologies and thickness measurements of the samples show that RTA can improve crystal quality, while increasing the thickness of the surface roughness layer due to partial surface decomposition in the process of thermal annealing.

**Keywords:** spectroscopic ellipsometry; optical properties; temperature; Be-implanted GaN

## 1. Introduction

Gallium nitride (GaN) based semiconductor materials have drawn intensive attention for a long time due to its some advantages of the large bandgap, high thermal conductivity and stable chemical properties. It has been extensively used in high-temperature power devices, high-frequency microwave devices and light-emitting diodes [1–4]. These devices are typically achieved by p-type and n-type doping in metal–organic chemical vapor deposition (MOCVD) process [5–11]. Nitride materials are usually doped with silicon (Si) or magnesium (Mg) to form n-type or p-type materials, respectively.

Si is capable of forming effective doping as a shallow donor in GaN, and its ionization energy and ionization electron concentration are around 35 meV and  $1 \times 10^{19} \text{ cm}^{-3}$ , respectively [12]. Pankove argued that Mg had a low activation of the acceptor at room temperature (RT) due to the large optical ionization energy which was about 250 meV [13]. However, the thermal ionization energy of p-type impurity doped Mg is 150–200 meV above the valence band, which is easily affected by the residual impurities in the material [10,14–16]. The ionization hole carrier concentration can reach more than  $1 \times 10^{18} \text{ cm}^{-3}$ , but it is hard to reach beyond  $1 \times 10^{20} \text{ cm}^{-3}$  [17]. The selective area doping can provide precise control of dopant concentration and depth distribution, which can be achieved by ion implantation for semiconductor devices. Meanwhile, implantation-induced damage removal and efficient activation of both p-type and n-type dopants are performed by high temperature rapid thermal annealing (RTA) [18]. However, it is formidable to obtain p-type conductivity at RT for Mg-implanted doping because implantation-induced damage may easily compensate the holes generated from Mg acceptors with heavy-ion mass and deep acceptor levels [19].

Beryllium (Be) which is an element of the same chemical family as Mg in the periodic table of elements, is the most promising candidate for p-type doping in GaN since its theoretical activation energy of 60 meV [20]. The studies showed that Be-doped GaN was slight p-type conductivity [21] because  $\text{Be}_{\text{Ga}}$  is a deep acceptor ( $E_{\text{V}} + 0.55 \text{ eV}$ ) [22]. The interesting behavior observed is that Be exhibits amphoteric behavior in GaN, involving switching between substitutional and interstitial positions in the lattice [23]. Ronning et al. studied the optical activation of undoped GaN after Be implantation and annealing, indicated the Be-related transition at 3.35 eV and defects related luminescence peak at 3.44 eV in the photoluminescence (PL) spectra measurement at 14 K [24]. The Be-related transition was also observed at 3.363 eV in PL spectra of pulsed laser annealing sample, but could not find it in the RTA sample [25]. The parallel results have been reported about Be-related emission detected by PL in Be-doped GaN grown by molecular beam epitaxy (MBE) [26,27]. Many studies have been conducted on Be implanted in undoped GaN [21,28]. Some studies revealed that minority carrier levels and majority carrier traps were detected in the 0.18–1.2 eV and 0.2–1.2 eV energy range in Be-implanted GaN epilayers [29,30]. In spite of Be being now considered for white light-emitting diodes (LEDs) or for achieving high resistivity GaN layers [23,31], there is no systematic exploration of optical properties of Be-implanted GaN, especially the change of refractive indices, extinction coefficients and bandgap at high temperature.

In this paper, a series of Be-implanted GaN thin films with different RTA processes were investigated by variable angle and temperature-dependent spectroscopic ellipsometry (SE). These optical properties were obtained in a spectral range of 200 to 1600 nm (6.2–0.77 eV). The unannealed sample was determined in the temperature range of 300–850 K. The cross-section microstructure and epilayer total thickness of films were determined by scanning electron microscope (SEM). Additionally, dual-beam ultraviolet-visible spectrophotometer (UV-VIS) was used to evaluate the crystal quality of thin films and the thickness of the epilayer. The surface morphology was characterized by atomic force microscopy (AFM). Moreover, Transport of ions in matter (TRIM) simulation was carried out to verify the mean depth of Be ion implantation.

## 2. Materials and Methods

The hexagonal structure GaN epilayers with a thickness of about 2  $\mu\text{m}$  were grown on (0001) sapphire substrates by using low-pressure metalorganic chemical vapor deposition (LPMOCVD) with trimethylgallium (TMGA) and ammonia ( $\text{NH}_3$ ) as the source precursors for Ga and N. The growth temperature for the GaN buffer and the single crystal epilayer was 600 °C and 1100 °C, respectively. During the LPMOCVD process, flow rates of TMG,  $\text{NH}_3$ , and  $\text{H}_2$  were 10  $\mu\text{mol}/\text{min}$ , 3.0  $\text{sl}/\text{min}$ , and 0.5  $\text{sl}/\text{min}$ , respectively, and reaction pressure in the chamber was 76 Torr. These GaN samples were subsequently implanted at RT by a dose of  $5 \times 10^{14} \text{ cm}^{-2}$  Be ions with an energy of 50 keV. After implantation, RTA was carried out for 40 s at temperature 600 °C, 900 °C and 1100 °C with  $\text{N}_2$  as the

ambient gas. To distinguish the details of each other, the implanted samples were named as follows,  $S_0$  (unannealed),  $S_1$  (RTA 600 °C),  $S_2$  (RTA 900 °C),  $S_3$  (RTA 1100 °C).

A dual rotating compensator Mueller matrix ellipsometer from Wuhan Eoptics Technology Co. Ltd., China, was utilized to obtain the ellipsometric data, while the temperature of samples was controlled with heating freezing stage system (THMS600). A continuous spectrum of incident radiation was emitted by the light source that composes by a deuterium lamp and a halogen lamp. SE measurements are considered as a non-destructive technique that can precisely measure optical constants, surface roughness and thickness of thin films. It is based on the measurement of the change in the polarization state, the ratio of amplitude ( $\psi$ ) and phase difference ( $\Delta$ ) of light upon reflection from the surface and the interface, and the utilization of the appropriate dispersion models to fit SE data. The SE experimental measurements were performed in a spectral range of 200–1600 nm (6.2–0.77 eV) with a step of 0.5 nm, at three different angles of incidence (50°, 60°, 70°) and the variable temperatures were determined by an embedded thermocouple with temperature interval 50 K of 300 to 850 K.

The CompleteEASE software (J.A. WoollamInc.) was used to fit experimental data and analysis optical constants, epilayers thickness and surface roughness of the Be-implanted GaN samples. The samples were exposed to air such a long time that the surface has formed a covering layer due to oxidation, contamination and other reasons. Therefore, the EMA/BeGaN/GaN/sapphire model structure was established to describe this material system. The surface roughness was defined as the average deviation from the mean surface height and described by the Bruggeman effective medium approximation (EMA). The surface roughness consists of 50/50 in an EMA between atmosphere and surface of BeGaN layer. The dielectric function of the sapphire substrate was provided by Adachi [32]. The BeGaN and GaN layers were described by Parametric Semiconductor oscillators (Psemi-M0 and Psemi-Tri) and Gaussian oscillators [33], as well as the epilayers dielectric functions can also be performed by these oscillators. The Parametric Semiconductor models, developed by Herzinger and Johs [34], have been successfully applied to fit the imaginary part of dielectric function ( $\epsilon_2$ ) critical point in direct bandgap semiconductors by combining a highly flexible functional shape and Kramers-Kronig consistency [33]. It is a crucial part of the SE data analysis process to quantify the exactness between the experimental data and the fitting data. The Mean Squared Error (MSE) is used to evaluate this exactness of fitting. It is universally acknowledged that the smaller value of MSE, the better would be the fitting between the measured SE data and the model data. The parameters of the oscillators in each epilayer were adjusted, until the SE parameters  $\psi$  and  $\Delta$  of bilayer model match the experimental SE data by using a regression fitting algorithm method.

UV-VIS was employed to measure optical transmission spectra in the wavelength region from 190 to 900 nm at RT. The spectra were recorded with a resolution of  $\lambda = 0.01$  nm and photometric accuracy of  $\pm 0.3\%$  for these optical transmittance measurements. AFM and SEM were used to obtain the film surface morphology and cross-section structural information, respectively. TRIM simulation was used for estimating the Be ion projection range of implanted GaN films.

### 3. Results and Discussion

#### 3.1. Microstructural Characterization

In order to confirm the thickness of films, the cross-section micrographs are determined by SEM. The Be-implanted GaN samples  $S_0$  and  $S_3$  are shown in Figure 1a,b, and the total thickness of epilayers were 2171.62 nm and 2151.81 nm, respectively. For unannealed sample  $S_0$ , it is obviously revealed that a sharp interface can be seen on the implantation surface with a thickness of 152.82 nm. With RTA at 1373 K, the sample  $S_3$ , however, an obvious interface under the same magnification is not observed. This can be interpreted as high-temperature RTA repairs the damage caused by Be ion implantation to regain the internal atomic redistribution after the implantation process. The AFM images of the above films are exhibited in Figure 2a,b, where the RMS surface roughness is obtained at 6.48 nm and 33.72 nm in the area of  $5 \mu\text{m} \times 5 \mu\text{m}$ , respectively. It can be observed that there is a dramatic difference

in the surface morphology between the unannealed sample and the RTA sample. Material bump in the direction perpendicular to the sample surface is a direct result of ion-beam-induced porosity of amorphous GaN, while large-scale surface roughness reflects the relief of stress associated with a lateral expansion of the amorphous GaN film [35,36]. Combined with the studied results of SEM, the AFM images provide a favorable characterization of the surface quality for the experimental samples.

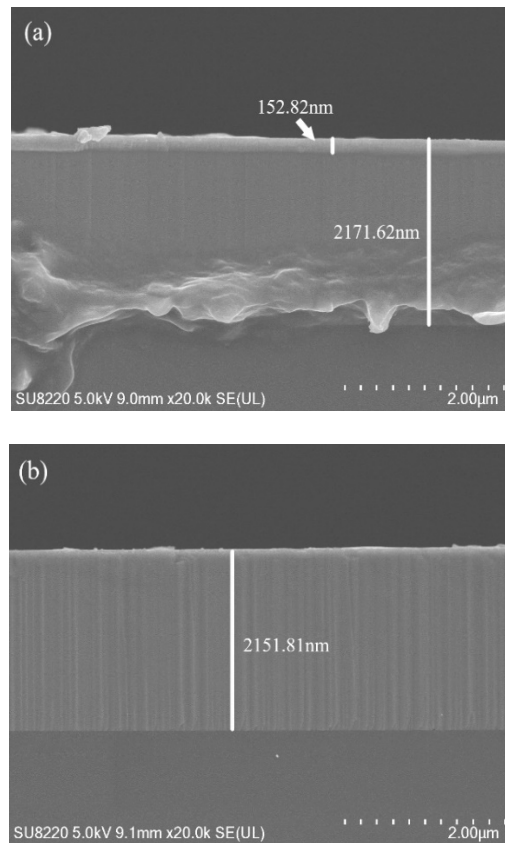


**Figure 1.** Scanning electron microscope (SEM) cross-section micrographs for Be-implanted gallium nitride (GaN) (BeGaN/GaN/sapphire model structure): (a) unannealed sample; (b) post-implantation rapid thermal annealing (RTA) at 1100 °C sample.

Figure 3 shows the optical transmission spectra of samples  $S_0$  and  $S_3$ . It is clearly seen from this figure that the sample  $S_0$  presented sluggish rising, but the sample  $S_3$  exhibited very sharp wavelength cutoff curves, indicating that the crystal quality of RTA sample  $S_3$  is better than that unannealed sample  $S_0$ . Due to the interference effect between GaN and sapphire substrate, the transmittance of samples in the UV-visible spectrum often reveals alternate maxima and minima in the long-wavelength range, and the thickness of samples can be obtained indirectly from the transmittance data of adjacent interference peaks. In the case of vertical incidence of light, the wavelengths corresponding to the adjacent maximum value of the interference part in the reflection spectrum are  $\lambda_1$  and  $\lambda_2$ , which are determined by the following equation:

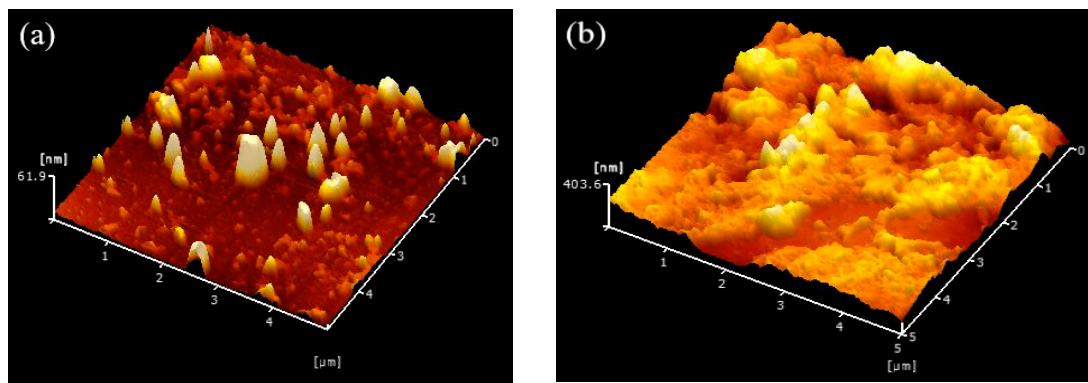
$$2n_1d = m\lambda_1 \quad (1)$$

$$2n_2d = (m + 1)\lambda_2, \quad (2)$$

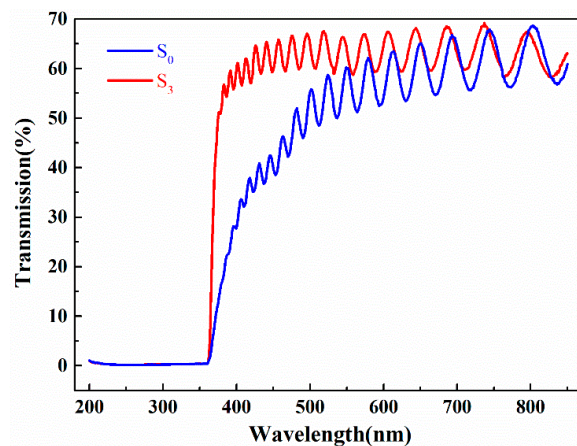
where  $n_1$  and  $n_2$  are the refractive indices of GaN with respect to the wavelength of  $\lambda_1$  and  $\lambda_2$ , respectively, and  $m$  stands for the series of interference peaks. The calculation formula of film thickness can be obtained from the above equation, expressing as [37]:

$$d = \lambda_1\lambda_2 / [2(n_1\lambda_2 - n_2\lambda_1)]. \quad (3)$$

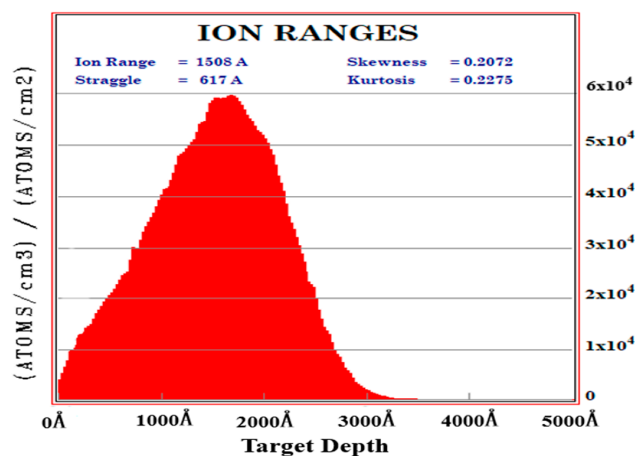
According to the above equations, we set  $n$  ( $n_1 = 2.40, n_2 = 2.39$ ) [38,39] and evaluated thin-film thickness by using adjacent interference peaks value near the wavelength of 600 nm. The mean values of film thickness for samples  $S_0$  and  $S_3$  can be reckoned at about 2183.1253 nm and 2166.2872 nm, respectively. The results are well consistent with SEM data. Furthermore, to investigate the mean depth of Be ion-implanted GaN, TRIM simulation is applied as a promising additional tool. Figure 4 shows the distribution of Be ions range in the GaN film for an ion beam energy of 50 keV. The mean depth of Be-implanted GaN is 150.80 nm, which is fairly close to the results of SEM (152.82 nm).



**Figure 2.** The three-dimensional atomic force microscopy (AFM) images of Be implanted GaN thin film: (a) unannealed sample; (b) post-implantation RTA at 1100 °C.



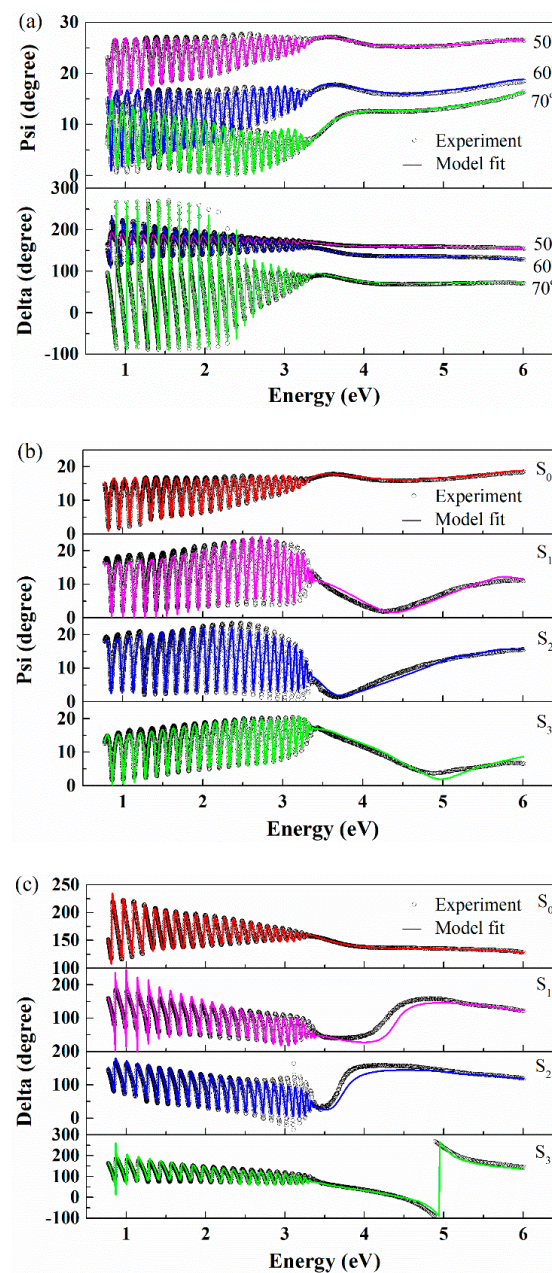
**Figure 3.** Optical transmission spectra of Be-implanted GaN sample unannealed (blue line) and post-implantation RTA at 1100 °C (red line).



**Figure 4.** The Be ion range distribution of 50 keV into GaN thin film.

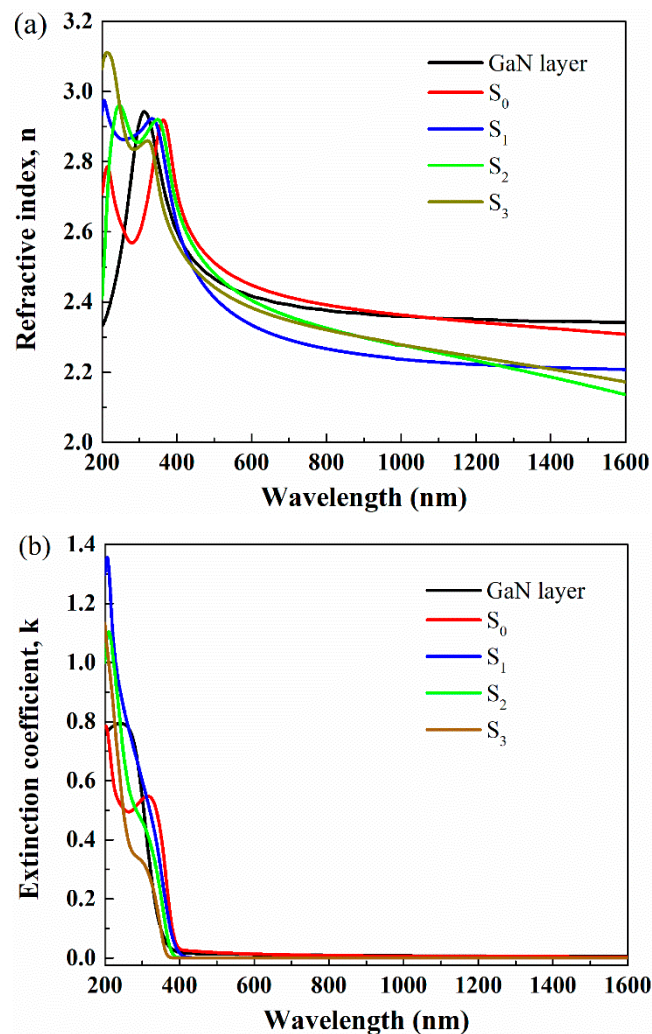
### 3.2. Optical Properties at Room Temperature

Figure 5a shows the best fitting results of ellipsometric spectra for Be-implanted GaN unannealed sample  $S_0$  at RT for three incident angles  $50^\circ$ ,  $60^\circ$  and  $70^\circ$ . SE experimental (dot lines) and model fitted (solid lines) for  $\psi$  and  $\Delta$  versus energy at incident angles  $60^\circ$  for four samples at RT are demonstrated in Figure 5b,c. As seen from these figures, the interference oscillations appeared below the bandgap corresponding to the transparent region of the sample, and the oscillations vanish above the bandgap. This difference appears due to the absorption of the incident light because of the interband transition. Following the  $S_0$ , the other samples have the same trends. In Table 1 the details of the thickness and surface roughness for thin films are described which have been gained by SE. The total thickness of GaN epilayers extracted from SE fitting agrees well with the values determined by SEM and UV-VIS.



**Figure 5.** Spectroscopic ellipsometry (SE) experimental (dot lines) and model fitted (solid lines)  $\psi$  and  $\Delta$  spectra vs energy plots: (a) three incident angles ( $50^\circ$ ,  $60^\circ$  and  $70^\circ$ ) of Be implanted GaN sample  $S_0$  at room temperature (RT); (b) and (c) are psi and delta with incident angle  $60^\circ$  for four samples at RT, respectively.

The refractive index ( $n$ ) and the extinction coefficient ( $k$ ) of Be-implanted GaN at RT are shown in Figure 6. As it is based on the GaN epilayer implantation experiment, in order to better illustrate the variation before and after implantations that we have listed the relevant data of the pristine GaN in Figure 6. As increasing the annealing temperature, there is a blueshift in the refractive index. The extinction coefficient of the samples moves towards the high-energy direction with the increase of annealing temperature. In a certain annealing temperature range, the increase of annealing temperature is beneficial to the blueshift of optical constants ( $n$  and  $k$ ). Compared to the hexagonal structure GaN, the value of  $k$  in the low-energy part has a larger value than that Be implanted layer; whereas the value of  $n$  for GaN has the highest value about the first turning point. There were three peaks ( $E_1$ ,  $E_2$ , and  $E_3$ ) in  $\epsilon_2(\omega)$  above the absorption edge in the energy range of 3–9.8 eV [40]. The peaks were primarily caused by the Van Hove singularities in the projected joint density of single-particle states, and then the peak intensities were strongly dependent on the attractive electron-hole interaction. Kawashima [38] and Aleksandra [39] measured the  $n$  and  $k$  of GaN by using Adachi's model dielectric function (MDF) in the range of 1.5–10 eV, showing the consistent results which consisted of two CP's. For GaN, the peak of  $n$  at  $\sim 365$  nm was associated with interband transitions ( $E_0$  gaps) and exciton contributions. Yan et al. did not find a clear second peak in the range of 0.75–6.5 eV [41].



**Figure 6.** Fitted optical constants of Be implanted GaN samples at RT: (a) refractive index ( $n$ ) vs. wavelength; (b) extinction coefficient ( $k$ ) vs. wavelength.

**Table 1.** Thicknesses information of Be implantation into GaN from SE.

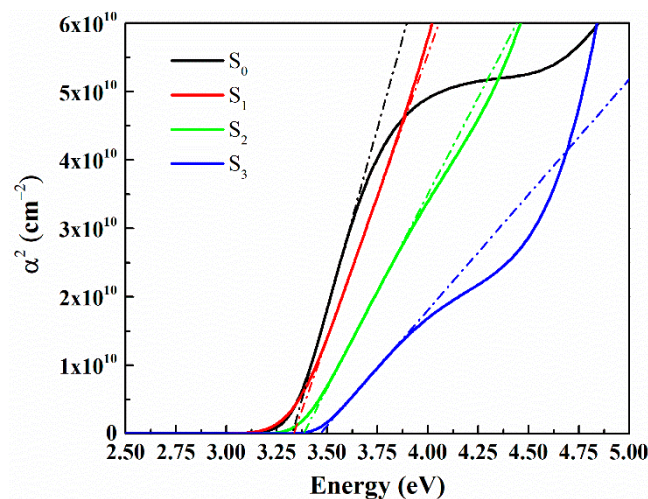
Sample	GaN Layer/nm	Implanted Layer/nm	Surface Roughness/nm
0#	1986.74 ± 2.26	148.37 ± 1.32	9.01 ± 0.11
1#	1978.67 ± 0.51	80.69 ± 0.47	47.50 ± 0.09
2#	1988.59 ± 1.12	84.22 ± 0.94	51.97 ± 0.24
3#	1997.18 ± 0.37	96.43 ± 0.35	41.40 ± 0.05

The optical absorption coefficient  $\alpha$  and bandgap  $E_g$  for direct band-gap materials can be obtained from the relations expressed by using Equations (4) and (5) [42,43].

$$\alpha = 4\pi k/\lambda \quad (4)$$

$$\alpha^2 = A(\hbar\nu - E_g), \quad (5)$$

where  $\lambda$  represents the wavelength,  $A$  indicates a constant. Hence, the bandgap  $E_g$  can be deduced from the variation of  $\alpha$  with  $\hbar\nu$ . The values of  $E_g$  can be calculated at the point of  $\alpha^2 = 0$  by linear fit close to the absorption edge, as shown in Figure 7. It can be observed that the  $E_g$  of samples are gradually increasing with the ascending annealing temperature. The bandgap  $E_g$  of the samples  $S_0$ – $S_3$  are 3.328 eV, 3.335 eV, 3.383 eV and 3.468 eV, respectively. The previous studies showed that one new line in the PL spectra at 3.35 eV provided strong evidence for the presence of optically active Be acceptors and had been assigned to band-acceptor recombination [24]. In addition, the similar results of Be-related emission were detected by PL in Be-implanted [25,28] and Be-doped [26,27] GaN sample. Since the structural damage is mostly repaired by high-temperature RTA, the defect will no longer be the main factor affecting the optical properties [44]. The bandgap values of sample  $S_2$  and  $S_3$  are very close to each other. The unannealed sample  $S_0$  has a minimum bandgap value of 3.328 eV, and the annealing temperature of the highest 1100 °C sample  $S_3$  presents the maximum bandgap value of 3.468 eV. The bandgap difference between sample  $S_0$  and sample  $S_3$  is only 140 meV. Different annealing temperature has little effect on the bandgap of Be implanted layers. It manifests that in GaN, interstitial Be undergoes a type of transient-enhanced diffusion until excess point defects are removed by annealing, at which stage the Be is basically immobile [45]. With the increase of annealing temperature, crystal ordering increases and the defects reduce gradually, giving rise to a change of energy of electronic transition that intrigues the increment of the bandgap. The redshift of band edge can also be observed in samples of different annealing temperatures. This redshift phenomenon can be explained as the internal damage caused by ion implantation which will be effectively reduced by RTA, so that partly Be ion can replace Ga site into the lattice and realize reordering.

**Figure 7.** The  $\alpha^2$  vs. energy for Be implanted GaN samples at RT.

### 3.3. Study on Variable Temperature SE

The SE spectra of unannealed sample  $S_0$  in the temperature range from 300 K to 850 K are discussed, where all SE experimental data are measured at the variable angles of  $50^\circ$ ,  $60^\circ$  and  $70^\circ$ . The refractive indices ( $n$ ) and extinction coefficients ( $k$ ) as a function of photon energy from 200 to 1600 nm can be obtained from the  $\psi$  and  $\Delta$  data at different temperatures as shown in Figure 8. The inset of Figure 8a,b display the change of optical constants causing by temperature. It is clearly revealed that the full width at half maximum of refractive index peaks tends to increase in the range of 300–450 nm. There is a redshift for the refractive index in the region of variable temperature. There is an absorption tail below bandgap for extinction coefficients attribute to the existence of defect states and impurities. The overall trend of refractive indices and extinction coefficients decrease and redshift as the temperature increase. That is, the  $n$  and  $k$  have maximum values towards the shorter wavelength region (high energy region) when the temperature changes from 300 to 850 K. The main reason for this phenomenon is that the bandgap of semiconductor materials changes with temperature. This behavior can be accounted for the increase in interatomic spacing when the amplitude of the atomic vibrations increases due to the increase of thermal energy. An increased interatomic spacing decreases the potential of the electrons in the material, which in turn reduces the bandgap. It means that applying high compressive (tensile) stress also causes an increase (decrease) of the bandgap. Furthermore, this effect of increasing bandgap may also cause by the lattice expansion of a material. The temperature dependence of the bandgap has been first proposed by Varshni by following expression for bandgap  $E_g$  as a function of the temperature  $T$  [46]:

$$E_g(T) = E_g(0) - \frac{aT^2}{T + b}, \quad (6)$$

where  $E_g(0)$  is the bandgap at  $T = 0$  K while  $a$  and  $b$  are constant parameters by fitting.

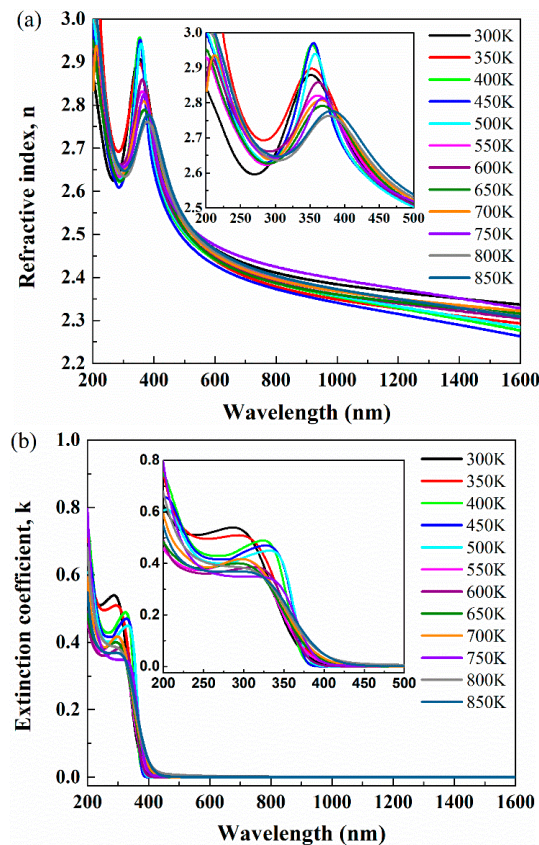


**Figure 8.** Fitted optical constants of sample  $S_0$  with temperature varied from 300 K to 850 K: (a) refractive index vs. wavelength; (b) extinction coefficient vs. wavelength.

Using the Equation (5), the optical bandgap is calculated from the square of absorption coefficient  $\alpha^2$  vs. photon energy with temperature varied from 300 K to 850 K, as demonstrated in Figure 9. The values of the bandgap  $E_0$  are gained from a linear fit, indicating a feature of shifting to the lower energy (red-shift) with increasing temperature. The change of bandgap  $E_0$  is in excellent agreement with refractive indices and extinction coefficients. The bandgap decreases with the rise of temperature and is exhibited in Figure 10, which is in good agreement with Equation (6). The value of bandgap reduces from 3.328 eV to 3.083 eV in the temperature range of 300–850 K. The decrease of bandgap with increasing temperature is generally contributed to two factors: (i) the lattice thermal expansion and (ii) the change of the acoustic and optic phonons involved electron-phonon interactions [44,47,48].

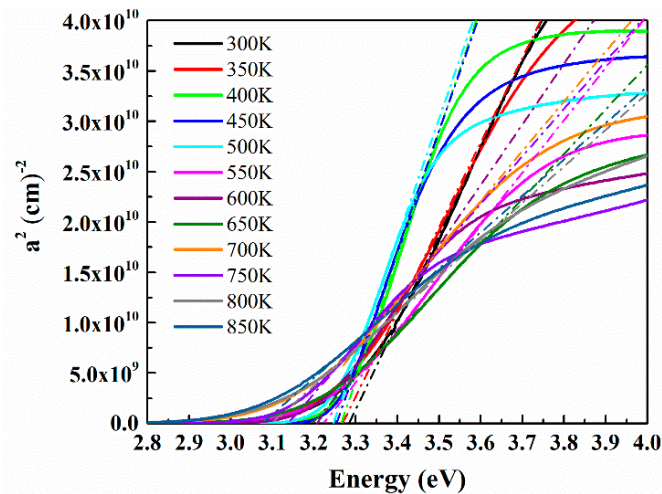


**Figure 9.** The square of the absorption coefficient ( $\alpha^2$ ) vs. photon energy at different temperature for sample  $S_0$ .

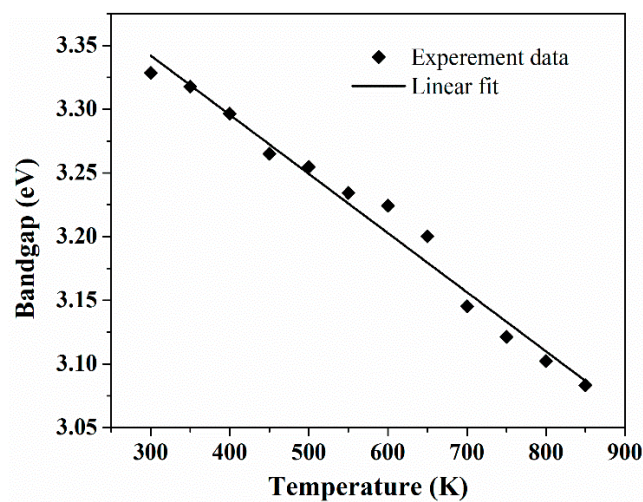


**Figure 10.** The bandgap values vs. temperature of sample  $S_0$  at 300 K–850 K.

#### 4. Conclusions

The influence of annealing temperature on optical properties of Be implanted GaN layers are investigated by spectroscopic ellipsometry. The surface morphologies and thickness of the samples imply that annealing can improve crystal quality but increase the thickness of the surface roughness layer. The mean depth of Be ion-implanted GaN can be given by TRIM simulation and SE fitting. With the increase of annealing temperature, the refractive index peak is found to shift from 368.0 nm to 317.5 nm and the extinction coefficient moves towards the high-energy region. The bandgap  $E_g$  of the samples  $S_0$ – $S_3$  are 3.328 eV, 3.335 eV, 3.383 eV and 3.468 eV respectively, at room temperature.

In a certain annealing temperature range of 873–1373 K, the refractive index, extinction coefficient and bandgap of the samples move towards the high-energy direction (blue shift) with the increase of annealing temperature. For the unannealed sample  $S_0$ , the value of bandgap varies from 3.328 eV to 3.083 eV in the temperature range of 300–850 K. The bandgap  $E_g$  exhibits redshift with increasing temperature, which is generally explained to the lattice thermal expansion and electron-phonon interactions. This can provide the way for developing devices in high temperature, high power and high-frequency microwave regions; hence, we conduct variable temperature SE to take the change of refractive index, extinction coefficient and bandgap at high temperature as an important reference in application.

**Author Contributions:** Conceptualization, W.W. and W.S.; methodology, J.W., Y.L. and Y.P.; software, J.W. and Y.L.; validation, Y.L. and M.M.; formal analysis, W.W.; investigation, W.W.; resources, W.S. and Y.W.; data curation, Y.P. and B.P.; writing—original draft preparation, W.W.; writing—review and editing, W.S., W.W., and M.M.; visualization, B.P.; supervision, Y.W.; project administration, W.S.; funding acquisition, W.S. and Y.W. All authors have been read and agreed to the published version of the manuscript.

**Funding:** This work was supported in part by the funding (Nos. T31200992001 and T3120097921) for the Bagui Talent of Guangxi province, ASEAN Young Talented Scientist Program (No. Y312001913), talent model base (No. AE31200065) and Guangxi Science and Technology Program (AD19245132), China.

**Conflicts of Interest:** The authors declare no conflict of interest.

## References

- Nakamura, S.; Senoh, M.; Nagahama, S.-I.; Iwasa, N.; Yamada, T.; Matsushita, T.; Kiyoku, H.; Sugimoto, Y.; Kozaki, T.; Umemoto, H.; et al. InGaN/GaN/AlGaIn-Based Laser Diodes With Modulation-Doped Strained-Layer Superlattices Grown on an Epitaxially Laterally Overgrown GaN Substrate. *Appl. Phys. Lett.* **1998**, *72*, 11–213. [[CrossRef](#)]
- Zhang, A.P.; Johnson, J.W.; Ren, F.; Han, J.; Polyakov, A.; Smirnov, N.B.; Govorkov, A.V.; Redwing, J.M.; Lee, K.; Pearton, S.J. Lateral Al<sub>x</sub>Ga<sub>1-x</sub>N Power Rectifiers With 9.7 KV Reverse Breakdown Voltage. *Appl. Phys. Lett.* **2001**, *78*, 823–825. [[CrossRef](#)]
- Teisseyre, H.; Bockowski, M.; Grzegory, I.; Kozanecki, A.; Damilano, B.; Zhydashvsky, Y.; Kunzer, M.; Holc, K.; Schwarz, U. GaN Doped With beryllium—An Effective Light Converter for White Light Emitting Diodes. *Appl. Phys. Lett.* **2013**, *103*, 11107. [[CrossRef](#)]
- Leute, R.A.R.; Wang, J.; Meisch, T.; Biskupek, J.; Kaiser, U.; Scholz, F. Blue to True Green LEDs With Semipolar Quantum Wells Based on GaN Nanostripes. *Phys. Status Solidi c* **2015**, *12*, 376–380. [[CrossRef](#)]
- Goldenberg, B.; Zook, J.D.; Ulmer, R.J. Ultraviolet and Violet Light-Emitting GaN Diodes Grown by Low-Pressure Metalorganic Chemical Vapor Deposition. *Appl. Phys. Lett.* **1993**, *62*, 381–383. [[CrossRef](#)]
- Lin, M.E.; Greene, J.E.; Morkoç, H.; Xue, G.; Zhou, G.L. p-type zinc-Blende GaN on GaAs Substrates. *Appl. Phys. Lett.* **1993**, *63*, 932–933. [[CrossRef](#)]
- Wang, C.; Davis, R.F. Deposition of Highly Resistive, Undoped, and P-Type, Magnesium-Doped Gallium Nitride Films by Modified Gas Source Molecular Beam Epitaxy. *Appl. Phys. Lett.* **1993**, *63*, 990–992. [[CrossRef](#)]
- Kim, J.G.; Frenkel, A.C.; Liu, H.; Park, R.M. Growth by Molecular Beam Epitaxy and Electrical Characterization of Si-doped Zinc Blende GaN Films Deposited on  $\beta$ -SiC Coated (001) Si Substrates. *Appl. Phys. Lett.* **1994**, *65*, 91–93. [[CrossRef](#)]
- Molnar, R.J.; Moustakas, T.D. Growth of Gallium Nitride by Electron-Cyclotron Resonance Plasma-Assisted Molecular-Beam Epitaxy: The Role of Charged Species. *J. Appl. Phys.* **1994**, *76*, 4587–4595. [[CrossRef](#)]
- Rubin, M.; Newman, N.; Chan, J.S.; Fu, T.C.; Ross, J.T. P-Type Gallium Nitride by Reactive Ion-Beam Molecular Beam Epitaxy With Ion Implantation, Diffusion, or Coevaporation of Mg. *Appl. Phys. Lett.* **1994**, *64*, 64–66. [[CrossRef](#)]
- Abernathy, C.R.; MacKenzie, J.D.; Pearton, S.J.; Hobson, W.S. CCl<sub>4</sub> Doping of GaN Grown by Metalorganic Molecular Beam Epitaxy. *Appl. Phys. Lett.* **1995**, *66*, 1969–1971. [[CrossRef](#)]
- Lisker, M.; Witte, H.; Krtschil, A.; Christen, J.; As, D.J.; Schöttker, B.; Lischka, K. Enhancement of UV-Sensitivity in GaN/GaAs Heterostructures by Si-Doping. *Mater. Sci. Forum* **2000**, *338*, 1591–1594. [[CrossRef](#)]

13. Pankove, J.I.; Hutchby, J.A. Photoluminescence of ion-implanted GaN. *J. Appl. Phys.* **1976**, *47*, 5387–5390. [[CrossRef](#)]
14. Tanaka, T.; Watanabe, A.; Amano, H.; Kobayashi, Y.; Akasaki, I.; Yamazaki, S.; Koike, M. p-type Conduction in Mg-doped GaN and Al<sub>0.08</sub>Ga<sub>0.92</sub>N Grown by Metalorganic Vapor Phase Epitaxy. *Appl. Phys. Lett.* **1994**, *65*, 593–594. [[CrossRef](#)]
15. Johnson, C.; Lin, J.Y.; Jiang, H.X.; Khan, M.A.; Sun, C.J. Metastability and Persistent Photoconductivity in Mg-doped p-type GaN. *Appl. Phys. Lett.* **1996**, *68*, 1808–1810. [[CrossRef](#)]
16. Seghier, D.; Gislason, H.P. Electrical Characterization of Mg-Related Energy Levels and the Compensation Mechanism in GaN:Mg. *J. Appl. Phys.* **2000**, *88*, 6483–6487. [[CrossRef](#)]
17. Albrecht, F.; Grillenberger, J.; Dietrich, M.; Reislöhner, U.; Hülsen, C.; Pasold, G.; Witthuhn, W.; the ISOLDE collaboration. Observation of a Be-Correlated Donor State in GaN. *Appl. Phys. Lett.* **2004**, *84*, 3876. [[CrossRef](#)]
18. Tan, H.H.; Williams, J.; Zou, J.; Cockayne, D.J.H.; Pearton, S.J.; Zolper, J.C.; Stall, R.A. Annealing of Ion Implanted Gallium Nitride. *Appl. Phys. Lett.* **1998**, *72*, 1190–1192. [[CrossRef](#)]
19. Kent, D.G.; Overberg, M.E.; Pearton, S.J. Co-Implantation of Be+O and Mg+O into GaN. *J. Appl. Phys.* **2001**, *90*, 3750–3753. [[CrossRef](#)]
20. Bernardini, F.; Fiorentini, V.; Bosin, A. Theoretical Evidence for Efficient P-Type Doping of GaN Using Beryllium. *Appl. Phys. Lett.* **1997**, *70*, 2990–2992. [[CrossRef](#)]
21. Nakano, Y.; Jimbo, T. Electrical Characterization of Acceptor Levels in Be-Implanted GaN. *Appl. Phys. Lett.* **2002**, *81*, 3990–3992. [[CrossRef](#)]
22. Lyons, J.L.; Janotti, A.; Van De Walle, C.G. Impact of Group-II Acceptors on the Electrical and Optical Properties of GaN. *Jpn. J. Appl. Phys.* **2013**, *52*, 8. [[CrossRef](#)]
23. Tuomisto, F.; Prozheeva, V.; Makkonen, I.; Myers, T.H.; Bockowski, M.; Teisseyre, H. Amphoteric Be in GaN: Experimental Evidence for Switching Between Substitutional and Interstitial Lattice Sites. *Phys. Rev. Lett.* **2017**, *119*, 196404. [[CrossRef](#)] [[PubMed](#)]
24. Ronning, C.; Carlson, E.P.; Thomson, D.B.; Davis, R.F. Optical Activation of Be Implanted into GaN. *Appl. Phys. Lett.* **1998**, *73*, 1622–1624. [[CrossRef](#)]
25. Wang, H.T.; Tan, L.S.; Chor, E.F. Pulsed Laser Annealing of Be-Implanted GaN. *J. Appl. Phys.* **2005**, *98*, 094901. [[CrossRef](#)]
26. Dewsnip, D.J.; Андрианов, A.; Harrison, I.; Orton, J.; E Lacklison, D.; Ren, G.B.; E Hooper, S.; Cheng, T.S.; Foxon, C. Photoluminescence of MBE Grown Wurtzite Be-Doped GaN. *Semicond. Sci. Technol.* **1998**, *13*, 500–504. [[CrossRef](#)]
27. Sanchez, F.J.; Calle, F.; Garcia, M.A.S.; Calleja, E.; Muñoz, E.; Molloy, C.H.; Somerford, D.J.; Koschnick, F.K.; Michael, K.; Spaeth, J.-M. Luminescence of Be-Doped GaN Layers Grown by Molecular Beam Epitaxy on Si (111). *MRS Internet J. Nitride Semicond. Res.* **1998**, *3*, e19. [[CrossRef](#)]
28. García, R.; Ramos-Carrasco, A.; Berman-Mendoza, D.; A Hirata, G.; Contreras, O.; Barboza-Flores, M. Photoluminescence Enhancement from GaN by Beryllium Doping. *Opt. Mater.* **2016**, *60*, 398–403. [[CrossRef](#)]
29. Alfieri, G.; Sundaramoorthy, V.K. Minority Carrier Traps in Ion-Implanted n-Type Homoepitaxial GaN. *Phys. Status Solidi b* **2020**, *257*. [[CrossRef](#)]
30. Alfieri, G.; Sundaramoorthy, V.K. Deep Level Study of Beryllium Implanted MOCVD Homoepitaxial GaN. *Jpn. J. Appl. Phys.* **2019**, *58*, SCCB04. [[CrossRef](#)]
31. Bockowski, M.; Fijalkowski, M.; Sochacki, T.; Amilusik, M.; Lucznik, B.; Iwinska, M.; Sidor, A.; Kamler, G.; Oklej, M.; Jakiela, R.; et al. Implantation of Beryllium into Thin Unintentionally Doped Layers of Gallium Nitride Crystallized by Halide Vapor Phase Epitaxy (Conference Presentation). *Gallium Nitride Mater. Devices XIV* **2019**, *10918*, 1091805. [[CrossRef](#)]
32. Adachi, S. *Properties of Group-IV, III-V and II-VI Semiconductors*; Wiley: Chichester, UK, 2005; pp. 753–754. [[CrossRef](#)]
33. Motamedi, P.; Cadien, K. Structural and Optical Characterization of Low-Temperature ALD Crystalline AlN. *J. Cryst. Growth* **2015**, *421*, 45–52. [[CrossRef](#)]
34. Herzinger, C.M.; Johs, B.; McGahan, W.A.; Woollam, J.A.; Paulson, W. Ellipsometric Determination of Optical Constants for Silicon and Thermally Grown Silicon Dioxide via a Multi-Sample, Multi-Wavelength, Multi-Angle Investigation. *J. Appl. Phys.* **1998**, *83*, 3323–3336. [[CrossRef](#)]
35. Kucheyev, S.; Williams, J.; Zou, J.; Jagadish, C.; Li, G. Ion-Beam-Induced Dissociation and Bubble Formation in GaN. *Appl. Phys. Lett.* **2000**, *77*, 3577–3579. [[CrossRef](#)]

36. Kucheyev, S.; Williams, J.; Zou, J.; Jagadish, C.; Li, G. High-Dose Ion Implantation into GaN. *Nucl. Instrum. Methods Phys. Res. Sect. B Beam Interact. Mater. At.* **2001**, *175*, 214–218. [[CrossRef](#)]
37. Manificier, J.C.; Gasiot, J.; Fillard, J.P. A Simple Method for the Determination of the Optical Constants N, K and the Thickness of a Weakly Absorbing Thin Film. *J. Phys. E Sci. Instrum.* **1976**, *9*, 1002–1004. [[CrossRef](#)]
38. Kawashima, T.; Yoshikawa, H.; Adachi, S.; Fuke, S.; Ohtsuka, K. Optical Properties of Hexagonal GaN. *J. Appl. Phys.* **1997**, *82*, 3528–3535. [[CrossRef](#)]
39. Djurišić, A.B.; Li, E.H. Modeling the Optical Constants of Hexagonal GaN, InN, and AlN. *J. Appl. Phys.* **1999**, *85*, 2848–2853. [[CrossRef](#)]
40. Benedict, L.; Wethkamp, T.; Wilmers, K.; Cobet, C.; Esser, N.; Shirley, E.L.; Richter, W.; Cardona, M. Dielectric Function of Wurtzite GaN and AlN Thin Films. *Solid State Commun.* **1999**, *112*, 129–133. [[CrossRef](#)]
41. Yan, C.H.; Yao, H.; Van Hove, J.M.; Wowchak, A.M.; Chow, P.P.; Zavada, J.M. Ordinary Optical Dielectric Functions of Anisotropic Hexagonal GaN Film Determined by Variable Angle Spectroscopic Ellipsometry. *J. Appl. Phys.* **2000**, *88*, 3463–3469. [[CrossRef](#)]
42. Fujiwara, H. *Introduction to Spectroscopic Ellipsometry*; Wiley: Chichester, UK, 2007; pp. 1–11. [[CrossRef](#)]
43. Sohal, S.; Feng, W.; Pandikunta, M.; Kuryatkov, V.V.; Nikishin, S.; Holtz, M. Influence of Phonons on the Temperature Dependence of the Band Gap of AlN and Al<sub>x</sub>Ga<sub>1-x</sub>N Alloys With High AlN Mole Fraction. *J. Appl. Phys.* **2013**, *113*, 43501. [[CrossRef](#)]
44. Liu, X.; Li, B. IR Variable Angle Spectroscopic Ellipsometry Study of High Dose Ion-Implanted and Annealed Silicon Wafers. *J. Appl. Phys.* **2009**, *105*, 13533. [[CrossRef](#)]
45. Kucheyev, S.; Williams, J.; Pearton, S.J. Ion Implantation into GaN. *Mater. Sci. Eng. R Rep.* **2001**, *33*, 51–108. [[CrossRef](#)]
46. Varshni, Y. Temperature Dependence of the Energy Gap in Semiconductors. *Physica* **1967**, *34*, 149–154. [[CrossRef](#)]
47. Choi, S.; Kim, T.; Hwang, S.; Li, J.; Persson, C.; Kim, Y.; Wei, S.-H.; Repins, I. Temperature Dependent Band-Gap Energy for Cu<sub>2</sub>ZnSnSe<sub>4</sub>: A Spectroscopic Ellipsometric Study. *Sol. Energy Mater. Sol. Cells* **2014**, *130*, 375–379. [[CrossRef](#)]
48. Liu, Y.; Li, Q.X.; Wan, L.Y.; Kucukgok, B.; Ghafari, E.; Ferguson, I.T.; Zhang, X.; Wang, S.; Feng, Z.C.; Lu, N. Composition and Temperature Dependent Optical Properties of Al<sub>x</sub>Ga<sub>1-x</sub>N Alloy by Spectroscopic Ellipsometry. *Appl. Surf. Sci.* **2017**, *421*, 389–396. [[CrossRef](#)]



© 2020 by the authors. Licensee MDPI, Basel, Switzerland. This article is an open access article distributed under the terms and conditions of the Creative Commons Attribution (CC BY) license (<http://creativecommons.org/licenses/by/4.0/>).